Cytotherapy 000 (2023) 1–8

Contents lists available at ScienceDirect

CYTOTHERAPY

journal homepage: www.isct-cytotherapy.org

International Society ISCT Cell & Gene Therapy®

Short Report

Stromal Cell Therapy

Serum starvation affects mitochondrial metabolism of adipose-derived stem/stromal cells

Chiara Giannasi[1,2], Stefania Niada[2,*], Elena Della Morte[2], Silvia Rosanna Casati[3], Clara De Palma[3], Anna Teresa Brini[1,2]

[1] *Department of Biomedical Surgical and Dental Sciences, University of Milan, Milan, Italy*
[2] *IRCCS Istituto Ortopedico Galeazzi, Milan, Italy*
[3] *Department of Medical Biotechnology and Translational Medicine, University of Milan, Milan, Italy*

ARTICLE INFO

Article History:
Received 4 July 2022
Accepted 12 March 2023
Available online xxx

Key Words:
mesenchymal stromal cell
metabolomics
mitochondria
oxygen consumption rate
secretome
serum deprivation
serum-free

ABSTRACT

Background aims: A large part of mesenchymal stromal cell (MSC) regenerative and immunomodulatory action is mediated by paracrine signaling. Hence, an increasing body of evidence acknowledges the potential of MSC secretome in a variety of preclinical and clinical scenarios. Mid-term serum deprivation is a common approach in the pipeline of MSC secretome production. Nevertheless, up to now, little is known about the impact of this procedure on the metabolic status of donor cells.
Methods: Here, through untargeted differential metabolomics, we revealed an impairment of mitochondrial metabolism in adipose-derived MSCs exposed for 72 h to serum deprivation.
Results: This evidence was further confirmed by the significant accumulation of reactive oxygen species and the reduction of succinate dehydrogenase activity. Probably as a repair mechanism, an upregulation of mitochondrial superoxide dismutase was also induced.
Conclusions: Of note, the analysis of mitochondrial functionality indicated that, despite a significant reduction of basal respiration and ATP production, serum-starved MSCs still responded to changes in energy demand. This metabolic phenotype correlates with the obtained evidence of mitochondrial elongation and branching upon starvation.

Introduction

In 2001, a first work was published that described the presence of a population of mesenchymal stromal cells (MSCs) in human adipose tissue, with promising implications for cell-based therapy [1]. The last 20 years have witnessed a large number of scientific publications investigating the features and the therapeutic potential of adipose-derived MSCs (ASCs). Currently, more than 10 000 papers describe ASC action in disparate preclinical models, both *in vitro* and *in vivo* (source https://pubmed.ncbi.nlm.nih.gov/). Moreover, more than 200 clinical trials (https://clinicaltrials.gov/) have tested their therapeutic potential against diverse conditions, mostly affecting musculoskeletal and central nervous systems. As for MSCs in general, ASCs show a great immunomodulatory and regenerative potential [2,3] that strongly correlates with their ability to modulate the local microenvironment through paracrine signaling [4]. Over the last decade, the role of MSC secretome (or conditioned medium, CM) has emerged as a convenient alternative to cell therapy. CM consists of the plentitude of soluble and vesicle-conveyed factors secreted by the cells both *in vivo* and *in vitro*. As easily conceivable, during *in vitro* culture one can intervene on a great number of variables that strongly influence cell secretion. For example, the impact on secretome composition of different pre-conditioning strategies, such as hypoxia, inflammatory cues, and three-dimensional culture, has been recently reviewed [5,6]. Surprisingly, up to now the effects of mid-term serum deprivation, a common approach in the pipeline of secretome production, have been only marginally addressed. The advantages of animal serum removal upon secretome collection include reducing the risk of zoonosis and the onset of immunological or allergic reactions triggered by xenogeneic antigens. Furthermore, the exclusion of exogenous serum-derived soluble factors and extracellular vesicles (EVs) is particularly intriguing in the perspective of collecting cell secretome for therapeutic purposes. Finally, unlike other methods, serum deprivation does not require any further experimental procedures to eliminate the priming agent (e.g., inflammatory cytokines). Serum

* Correspondence: Stefania Niada, IRCCS Istituto Ortopedico Galeazzi, Via Galeazzi 4, 20161 Milan, Italy.
E-mail address: stefania.niada@grupposandonato.it (S. Niada).

https://doi.org/10.1016/j.jcyt.2023.03.004

deprivation impacts MSC immunomodulatory [7] and antitumoral [8] potency, alters the composition of EVs [9] and improves the release of trophic and angiogenic factors [10,11]. Moreover, this procedure stimulates vesiculation in several cell types, thus enhancing EV yield [12]. Furthermore, serum deprivation can also be used to modify the differentiation potential of MSCs in regenerative medicine approaches for several diseases, including musculoskeletal ones. Indeed, the reduction or even the lack of serum can improve MSC differentiation potential towards different cell phenotypes, such as the osteogenic [13] and the myocardial [14] ones. In addition, the gold standard protocols for chondrogenic differentiation conventionally exclude serum in the culture media. Serum starvation has obviously a great impact on the cell metabolism, and it most probably affects the composition and the action of cell secretome. We envision that a comprehensive understanding of the metabolic status of donor cells is relevant and advisable in the perspective of the clinical translation of cell secretome. In this work, we implemented an untargeted workflow for the differential analysis of metabolites between ASCs grown with 10% fetal bovine serum (FBS) and under serum deprivation. The evidence gained through metabolomics was then validated by *ad hoc* biochemical and functional assays in order to provide a proof of concept on the main pathways affected by serum withdrawal.

Materials and Methods

Cell cultures

ASCs were obtained from waste tissues collected at IRCCS Istituto Ortopedico Galeazzi upon institutional review board approval. In detail, cells were isolated from the subcutaneous adipose tissue of five patients (two male and three female, 61 ± 20 years of age) who underwent total hip arthroplasty (n = 4) or abdominoplasty (n = 1). At enrollment, all subjects were normo-weighted, with a body mass index lower than 30 and no documented diagnosis of obesity. Adipose tissue was shredded with a scalpel, digested with 0.75 mg/mL collagenase type I for 30 min at 37°C (Worthington Biochemical Corporation, Lakewood, NJ, USA) and filtered through a 100-μm cell strainer (Corning Incorporated, Corning, NY, USA). ASCs were plated at the density of 10^4/cm^2 in a standard culture medium (CTR medium) consisting of high-glucose Dulbecco's Modified Eagle's Medium supplemented with 10% FBS (FBS HyClone, Euroclone, Pero, Italy), 2 mmol/L glutamine, 50 μg/mL streptomycin and 50 U/mL penicillin. Cells were characterized for growth kinetics and multilineage differentiation following standard procedures (Supplementary Figure 1).

Preparation of pre- and post-starving samples

ASCs from IV to IX passage were employed for the experiments. At confluence, cells were either collected and stored/analyzed (CTR group) or rinsed twice with phosphate-buffered saline (PBS), washed for 1 h in a standard medium without FBS (serum-free medium, SF) then cultured for an additional 72 h in starving conditions (SF group) [15–22].

Metabolomics

Coupled pre- and post-starving cells (n = 3 donors, 6 × 10^6 ASCs/sample) were subjected to untargeted metabolomics for polar (amino acids, nucleotides and sugars) and apolar (fatty acids and membrane lipids) molecules at the Proteomics and Metabolomics Facility of IRCCS Ospedale San Raffaele (Milan, Italy). Samples were analyzed using the UPLC 1290 (Agilent Technologies, Milan, Italy) coupled to the TripleTOF 5600+ mass spectrometer (SCIEX, Framingham, MA, USA). Details on the confidential protocols are available upon reasonable request (https://research.hsr.it/en/core-facilities/promefa.html, facility manager Dr. Annapaola Andolfo, andolfo.annapaola@hsr.it).

Supplementary Table 2, Supplementary Table 3, Supplementary Table 4 and Supplementary Table 5 show the raw data of the known metabolites identified with the four columns. A total of 87 molecules were retained by removing duplicates. Of these, 77 metabolites were recognized by the web–based tool and were further considered for all the analyses (Supplementary Table 6). Unsupervised clustering (Pearson's distance), principal component analysis and metabolite set enrichment analysis were performed with MetaboAnalyst (www.metaboanalyst.ca).

Reactive oxygen species (ROS) assay

ROS were measured with the DCFDA/H2DCFDA – Cellular ROS Assay Kit (Abcam, Cambridge, UK) following the manufacturer's protocol. ASCs were plated in 96-well black clear bottom plates at the density of 4 × 10^3 cells/well. At confluence, pre-starving cells (CTR group) were analyzed whereas post-starving cells were shifted in serum-free medium and cultured for an additional 72 h (SF group). To summarize, cells were incubated with 30 μmol/L DCFDA (either in CTR or SF medium) for 45 min at 37°C in the dark, then fluorescence (Ex/Em = 485/535nm) was read with Wallac Victor II plate reader (Perkin Elmer, Milan, Italy). A positive oxidative stress control (cells treated with 125 μmol/L tert-butyl hydroperoxide for 4 h) was always included (data not shown).

Cell lysates and Western blotting

Pre- and post-starving cells were lysed with Lysis Buffer 6 (R&D Systems, Minneapolis, MN, USA) with 10 μg/mL aprotinin, 10 μg/mL leupeptin and 10 μg/mL pepstatin for 30 min at 4°C. Samples were centrifuged at 14 000*g* for 5 min, then the supernatants were collected and stored at −80°C. Total protein content was quantified through bicinchoninic acid assay (Thermo Fisher Scientific, Waltham, MA, USA). Then, 5 or 25 μg of proteins for each sample were loaded on 12% polyacrylamide gels or on 4–20% polyacrylamide precast gels (Criterion TGX Stain-free precast gels, Bio-Rad, Milan, Italy) and analyzed by sodium dodecyl-sulfate polyacrylamide gel electrophoresis and western blotting, using standard protocols. The mouse anti-SOD2 primary antibody (sc-137254, 1:500 diluted; Santa Cruz Biotechnology, CA, USA) and the mouse anti-DPR1 (611113, 1:1000 diluted; BD Biosciences, Franklin Lakes, NJ, USA) were incubated overnight at 4°C while the mouse anti-β-Actin primary antibody (A2228, Merck, Darmstadt, Germany, 1:5000 diluted) was incubated for 2 h at room temperature. Specific bands were revealed after the incubation with the appropriate secondary antibody conjugated to horseradish peroxidase (goat anti-mouse IgG, 62-6520, 1:6000 diluted; Thermo Fisher Scientific) followed by detection with ECL Westar Supernova (Cyanagen, Bologna, Italy). Signals were acquired by Chemidoc Imaging System and densitometry was quantified through Image Lab Software (Bio-Rad). To normalize the expression of target proteins, the band intensity of each sample was divided by the intensity of the loading control β-actin. For each population, post-starving data are expressed as relative values on the pre-starving group (CTR = 1).

3-[4,5-dimethylthiazol-2-yl]-2,5-diphenyltetrazolium bromide (MTT) assay

5 × 10^3 ASCs/well were cultured till confluence in 96-well tissue culture plates in standard medium (CTR medium). At confluence, ASCs were either tested (CTR group) or cultured for 72 additional hours in serum-free medium (SF group). Viability and metabolism of pre- and post-starving cells were assessed through MTT assay. After a

wash in PBS, cells were incubated in 0.5 mg/mL MTT (dissolved in the appropriate culture medium (CTR or SF medium) for 4 h at 37°C. Formazan precipitates were solubilized with 100% dimethyl sulfoxide and the absorbance was read at 550nm with Wallac Victor II plate reader (Perkin Elmer).

Analysis of mitochondrial network morphology

ASCs were seeded on 1-cm diameter glass coverslips at a density of $2 \times 10^4/cm^2$ and cultured till confluence. CTR and SF cells were incubated with 100 nmol/L Mitotracker (M7512; Invitrogen, Waltham, MA, USA) in the appropriate culture medium for 30 min at 37°C, then rinsed several times with PBS and fixed with 4% paraformaldehyde for 20 min at room temperature. Coverslips were mounted with ProLong Diamond Antifade Mountant with DAPI (Thermo Fisher Scientific). Images were acquired with Leica TCS SP8 AOBS microscope system using a 63× oil immersion objective (Leica Microsystems, Wetzlar, Germany) and analyzed using the plugin skeletonize (2D/3D) of Fiji software (ImageJ 1.52).

Mitochondrial respiration assessment

Mitochondrial oxygen consumption rate (OCR) was assessed with the Agilent Seahorse XFe24 Analyzer (Seahorse Bioscience; Agilent, Santa Carla, CA, USA) at the Advanced Technology Facility (Department of Biosciences, University of Milan, Milan, Italy). 2×10^4 ASCs were seeded into 24-well culture microplates (Agilent). Cells were tested after growing in standard medium (CTR group) or in serum-free medium for 72 h (SF group). Before analysis, cells were incubated for 1 h at 37°C at atmosphere with no CO_2 in pre-warmed unbuffered Dulbecco's Modified Eagle's Medium supplemented with 1 mmol/L pyruvate, 10 mmol/L glucose and 2 mol/L glutamine. OCR was measured using the Seahorse XF Cell Mito Stress Test Kit (103015-100; Agilent) following standard protocols. For the measurements, oligomycin (1.5 μmol/L), carbonyl cyanide-p-trifluoromethoxyphenylhydrazone (3 μmol/L) and rotenone/antimycin A (0.5 μmol/L) were added sequentially. The Seahorse software was used to plot the results. OCR values were normalized on cell count performed by nuclei staining with Hoechst 33342 followed by imaging with an ImageXpress Micro Confocal High Content Imaging System (Molecular Devices, San Jose, CA, USA) and automate cell counting with the MetaXpress Software (Molecular Devices) at the Advanced Technology Facility (Department of Biosciences, University of Milan, Milan, Italy).

Statistics

Statistical analysis was performed by paired or unpaired *t* test using Prism 9.2.0 (GraphPad Software, La Jolla, CA, USA). Differences were considered significant at P value ≤ 0.05.

Results

Serum deprivation, a common strategy for secretome production, allows cell priming [23] while avoiding the mixture of ASC-derived factors with exogenous ones. In this study, we focused on how this condition affects ASC metabolism. Our analyses were performed on sub-confluent ASCs, right before serum deprivation (CTR), and after 72 h of serum-free culture (SF). Standard cell features were not affected by the lack of serum for 72 h. In detail, cell morphology, cell-cycle progression and the expression of the typical MSC surface markers were never influenced (Supplementary Figure 7). In contrast, the metabolic profile was relevantly modified. The analysis of the 77 known metabolites, quantified in three different ASC populations before and after serum deprivation, revealed major differences. Indeed, unsupervised hierarchical clustering analysis distinctly discriminated between CTR and SF samples (Figure 1A) and principal component analysis confirmed the clear distinction between the two groups, with more than 80% of variance explained by factors 1 and 2 (Figure 1B).

Metabolite set enrichment analysis indicated several biologically relevant patterns significantly enriched and interconnected in our dataset (Figure 2A,B). Of note, almost all the metabolites involved in the patterns were less abundant in SF samples compared with CTR ones, thus suggesting an impairment of the corresponding metabolic processes upon serum deprivation (Supplementary Table 8).

In the top results, mitochondrial electron transport chain, oxidation of branched chain fatty acids and citric acid cycle (or tricarboxylic acid-TCA cycle) were the most relevant, due to the high number of metabolites involved (Figure 2C, Supplementary Table 8). Each process counts three hits, with succinic acid shared among all three pathways and fumaric acid shared between citric acid cycle and mitochondrial electron transport chain. Except for glycerophosphate, all of the other metabolites were significantly downregulated in post-starving samples with respect to pre-starving ones. These patterns are all associated with mitochondrial function.

Since one of the main consequences of mitochondrial impairment is the overproduction of ROS, we investigated this aspect. As assumed, ROS production was significantly increased during serum starvation (Figure 3A, +105% of CTR). At the same time, serum deprivation triggered an antioxidant response in ASCs, as revealed by the significant upregulation of mitochondrial superoxide dismutase 2 (SOD2) expression (Figure 3B, +413% of CTR), probably as a compensatory mechanism for ROS accumulation. The increased production of ROS matched with the significant reduction of succinate dehydrogenase activity after 72 h of serum starvation (Figure 3C, −47% of CTR), indicating an overall decrease of cell metabolic function. To better understand mitochondrial functionality, we measured OCR by Seahorse assay [24]. Under baseline conditions, SF ASCs present a lower energetic demand, leading to a significant reduction of basal and ATP-linked respiration (Figure 3D,E), and to a shift in the metabolic phenotype from aerobic/energetic to quiescent (Supplementary Figure 9). Conversely, when energy demand was mimicked (carbonyl cyanide-p-trifluoromethoxyphenylhydrazone injection), the differences in maximal respiration between CTR and SF cells become less evident (Figure 3D,E). As follows, the reserve capacity appears equal between groups, if not slightly higher in SF cells. This evidence suggests that, after serum starvation, ASCs retain their ability to adapt to metabolic changes. This could be coupled to changes in mitochondrial shape; therefore, we analyzed the levels of fission/fusion markers and mitochondrial network morphology in CTR and SF ASCs. Interestingly, the levels of the pro-fission GTPase dynamin-related protein-1 were significantly down modulated after serum starvation (Figure 3F, −24% of CTR), whereas other markers were not affected (Supplementary Figure 10). Consistently with dynamin-related protein-1reduction, the morphological analysis reveals a more complex and interconnected mitochondrial network in SF cells (Figure 3G), characterized by longer branches (Figure 3H), more junctions (Figure 3I) and fewer isolated ends (Figure 3L) with respect to CTR ones. Mitochondrial elongation during serum starvation can concur to the maintained functionality of these organelles and supports the evidence of a preserved fitness and flexibility of SF ASCs.

Discussion

MSCs are the first choice in most cell-based regenerative medicine approaches. Among different MSC sources, adipose tissue is particularly convenient in terms of harvesting procedures, cell yield and growth kinetics [25]. Lately, the scientific community has opened to the possibility of overcoming the ethical and practical drawbacks linked to MSC/ASC injection by harnessing the potential of their secretome. The depletion of animal components from culture medium is a crucial step in the pipeline of secretome production,

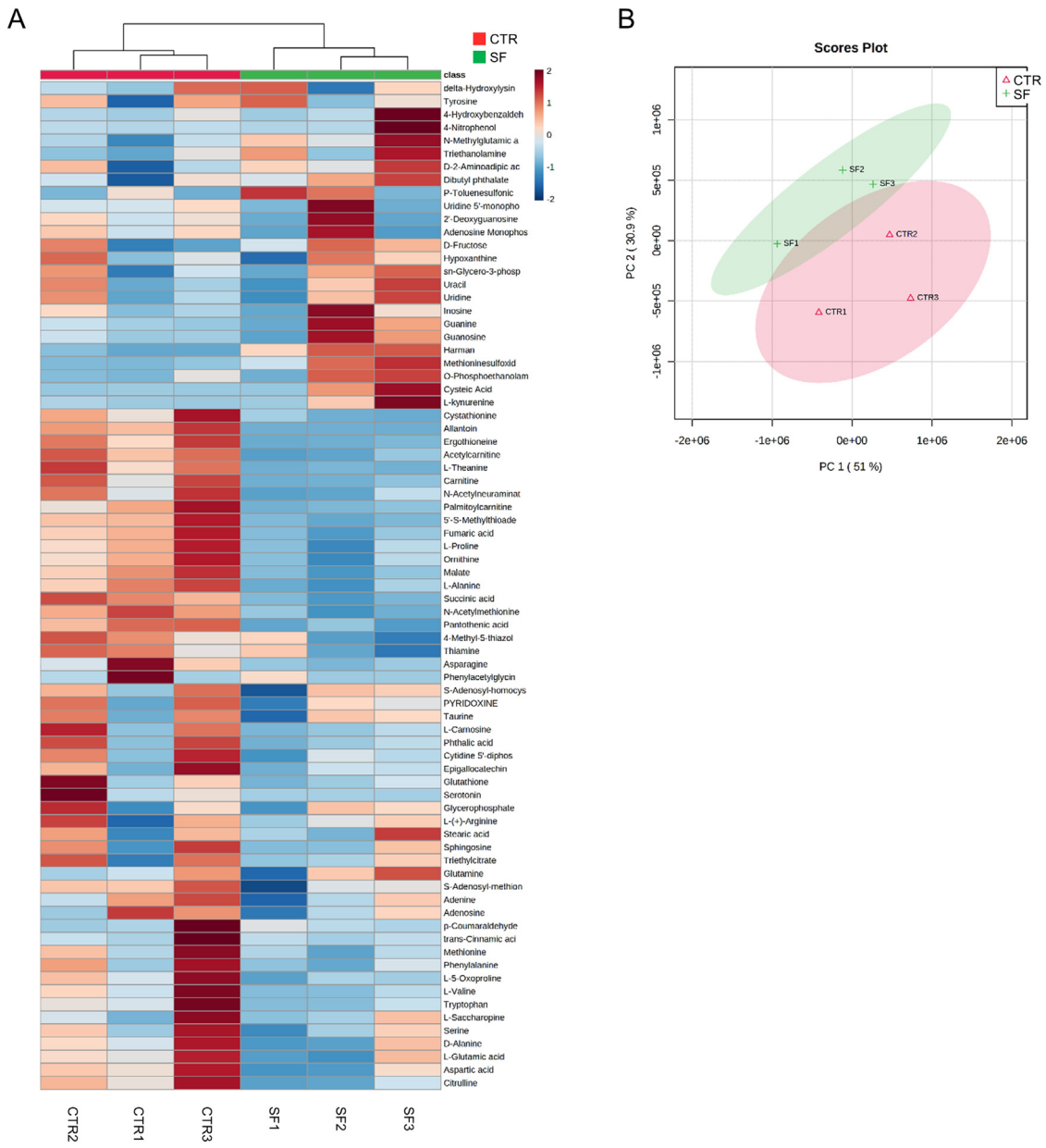

Fig. 1. Statistical analysis of metabolomics-derived datasets performed by MetaboAnalyst (www.metaboanalyst.ca). (A) Heatmap showing the unsupervised hierarchical clustering of control (CTR) and serum-free (SF) ASCs. The color scale (blue to red) represents the relative abundance of each metabolite. (B) Principal component analysis plot of the metabolic signatures of CTR (red triangles) and SF (green crosses) ASCs. Red and green ellipses show the clear clustering between groups. (For interpretation of the references to colour in this figure legend, the reader is referred to the web version of this article.)

especially when considering its future clinical translation. In recent years, several MSC culture media labelled as “xenofree” have been developed and patented. Unfortunately, their chemical composition is rarely disclosed. In cell-based approaches, these formulas present undeniable manufacturing advantages, which, however, wane in the perspective of a future clinical use of the secretome. Consequently, serum starvation still represents a very common strategy for secretome and/or EV collection. Here, we investigated how mid-term serum-free culture affects ASC features and their metabolic signature.

At first, we confirmed that serum starvation for 72 h did not affect ASC typical spindle-like and fibroblastic morphology, in agreement with previous evidence [26]. Furthermore, cell-cycle progression was not affected, even though its synchronization upon starvation has been previously described [27]. Of note, in our setting, the shift in serum-free medium was performed once cells reached a high degree of confluence. Consequently, the lack of difference between confluent ASCs grown in 10% FBS and starved cells may be due to cell-cycle arrest caused by contact inhibition (CI) [28]. Of note, during CI, cells do not undergo senescence and restore their proliferation rate upon detaching and replating [28]. In addition, serum deprivation did not affect ASC immunophenotype, as previously described in MSCs from Wharton’s jelly [29]. All these results together indicate that mid-term serum absence does not interfere on ASC basic properties.

The investigation of the metabolic signature of ASCs, pre- and post-starvation, was our main interest. Physiologically, cells respond to a nutrient-deficient microenvironment by either mobilizing endogenous substrates, triggering autophagy pathways or tuning mitochondrial metabolism [30]. It is well known that mitochondrial dynamics regulate many cell functions such as apoptosis, Ca^{++} transfer and cell-cycle progression [31]. As expected, nutrient withdrawal strongly affects cell metabolism. Indeed, a clear clustering between

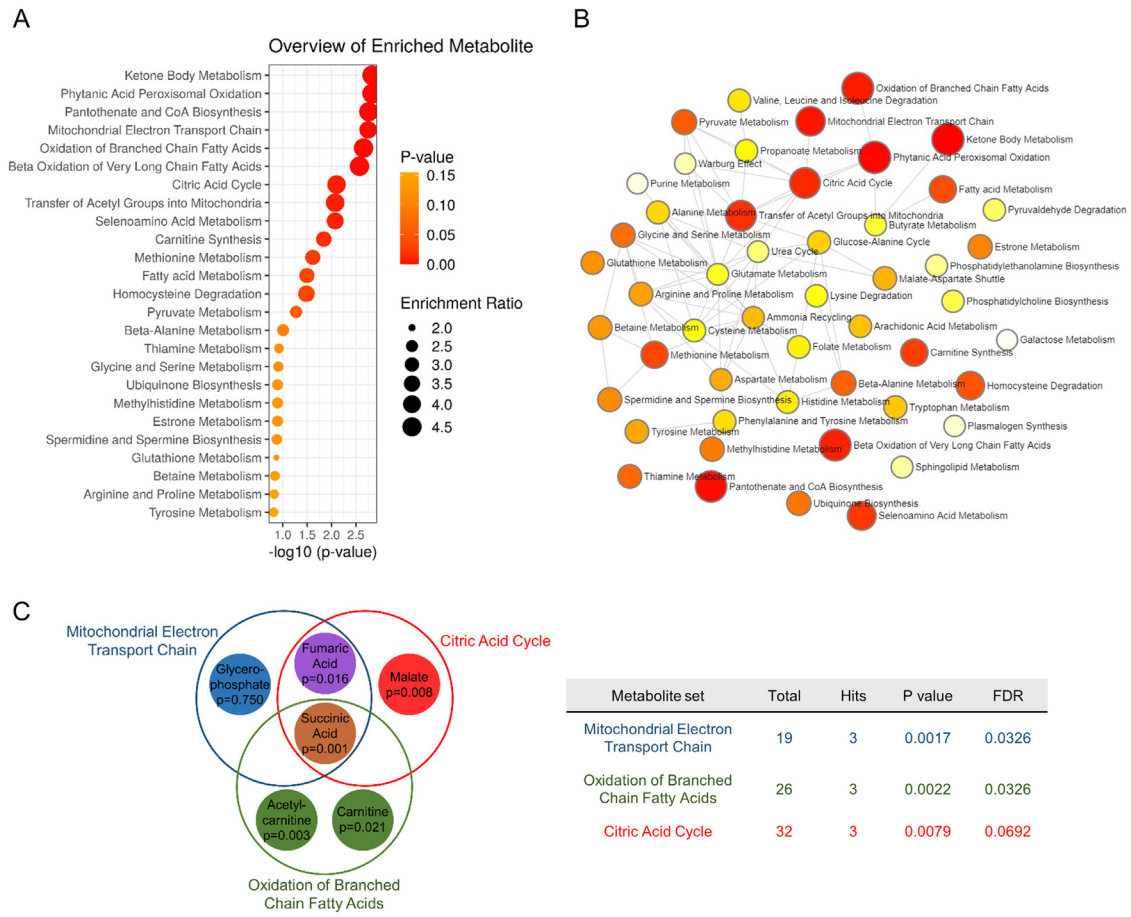

Metabolite set	Total	Hits	P value	FDR
Mitochondrial Electron Transport Chain	19	3	0.0017	0.0326
Oxidation of Branched Chain Fatty Acids	26	3	0.0022	0.0326
Citric Acid Cycle	32	3	0.0079	0.0692

Fig. 2. Quantitative enrichment analysis of metabolomics-derived datasets performed by MetaboAnalyst (www.metaboanalyst.ca). (A) Dot plot showing the overview of the top 25 enriched metabolite sets. The enrichment ratio is computed by Hits/Expected, where Hits are the observed hits and Expected are the expected ones. Dot dimension reflects the enrichment ratio (from 2.0 to 4.5) whereas the dot color (red to yellow) represents the *P* value. (B) Network view of all enriched metabolite sets. For each pathway, enrichment ratio and *P* value are visualized by dot dimension and color following the same scheme. (C) Graphical representation of the intersection between three significantly enriched pathways: mitochondrial electron transport chain (blue), oxidation of branched chain fatty acids (green) and citric acid cycle (red). The compound name for both shared and unshared hits is reported, together with the respective *P* value. The table summarizes the specifications of the processes, i.e., total number of components, hits, *P* value and false discovery rate (FDR). *P* values were calculated by paired *t*-test. (For interpretation of the references to colour in this figure legend, the reader is referred to the web version of this article.)

CTR and SF ASCs was obtained by untargeted metabolomics. Interestingly, of the 13 significantly different pathways (Supplementary Table 8), nine occur at least partially inside mitochondria.

Among the metabolites significantly influenced by serum starvation, succinic acid was identified in six different processes, consistently with its known localization at the crossroads of multiple metabolic pathways [32] (Figure 2C). Of note, succinic acid couples citric acid cycle (TCA) and the respiratory chain, two fundamental pathways for oxidative phosphorylation that were significantly impaired by serum starvation. Another hint of the impairment of these two processes was the significant reduction of succinate dehydrogenase activity (Figure 3C). This enzyme acts in both the TCA cycle and the electron transport chain. It links the oxidation of succinate to fumarate in the TCA cycle with the reduction of ubiquinone to ubiquinol in the electron transport chain, thus contributing to the maintenance of mitochondrial membrane potential and allowing ATP synthesis. The mitochondrial dysfunction that appears evident from this metabolomic analysis was confirmed by an increase in oxidative stress. ROS were significantly increased by serum deprivation (Figure 3A), consistently with other scientific evidences [33–35]. In our context, ASCs reacted to oxidative stress by increasing the expression of the enzymatic antioxidant SOD2 (Figure 3B). This is quite peculiar since a decrease of SOD1 and/or SOD2 expression has been observed during serum starvation in other cell types such as cardiomyocytes [36] or Wharton's jelly MSCs [29]. We might explain this with the known plasticity of adult MSCs and their ability to react to different stimuli.

Although oxidative stress does not induce positive effects on MSC physiology, its outcome on their CM is still controversial. Oxidative stress might induce the release of oxidized lipids and proteins. On the contrary, their secretome could include antioxidant molecules able to protect recipient cells by modulating their oxidative stress [37]. This last hypothesis agrees with our previous finding of SOD1 and SOD3 presence in the secretome of ASCs maintained in serum-free conditions for 72 h (supplementary Table 2 of Niada *et al.* [19]). The release of antioxidant molecules by ASCs under oxidative stress fits with the priming strategies largely investigated. The concept is to induce the same insult that cells would sense when injected *in vivo*, in order to modify their secretome by exploiting their plasticity. The evidence of a starvation-dependent mitochondrial impairment is further corroborated by the abundance of growth/differentiation factor 15, a recently validated biomarker of mitochondrial diseases [38], in the CM of serum-deprived ASCs (https://zenodo.org/record/5211269#.Yv9YRC7P1PY). Meanwhile, we obtained no clear results analyzing the intracellular expression of FGF21, a well-known marker of mitochondrial stress and functional defects [39] (Supplementary Figure 11). This discrepancy can be explained hypothesizing a modulation of FGF21 extracellular levels, since this mediator acts in an autocrine, paracrine and endocrine manner [40]. A more thorough analysis, evaluating at the same time intracellular and secreted

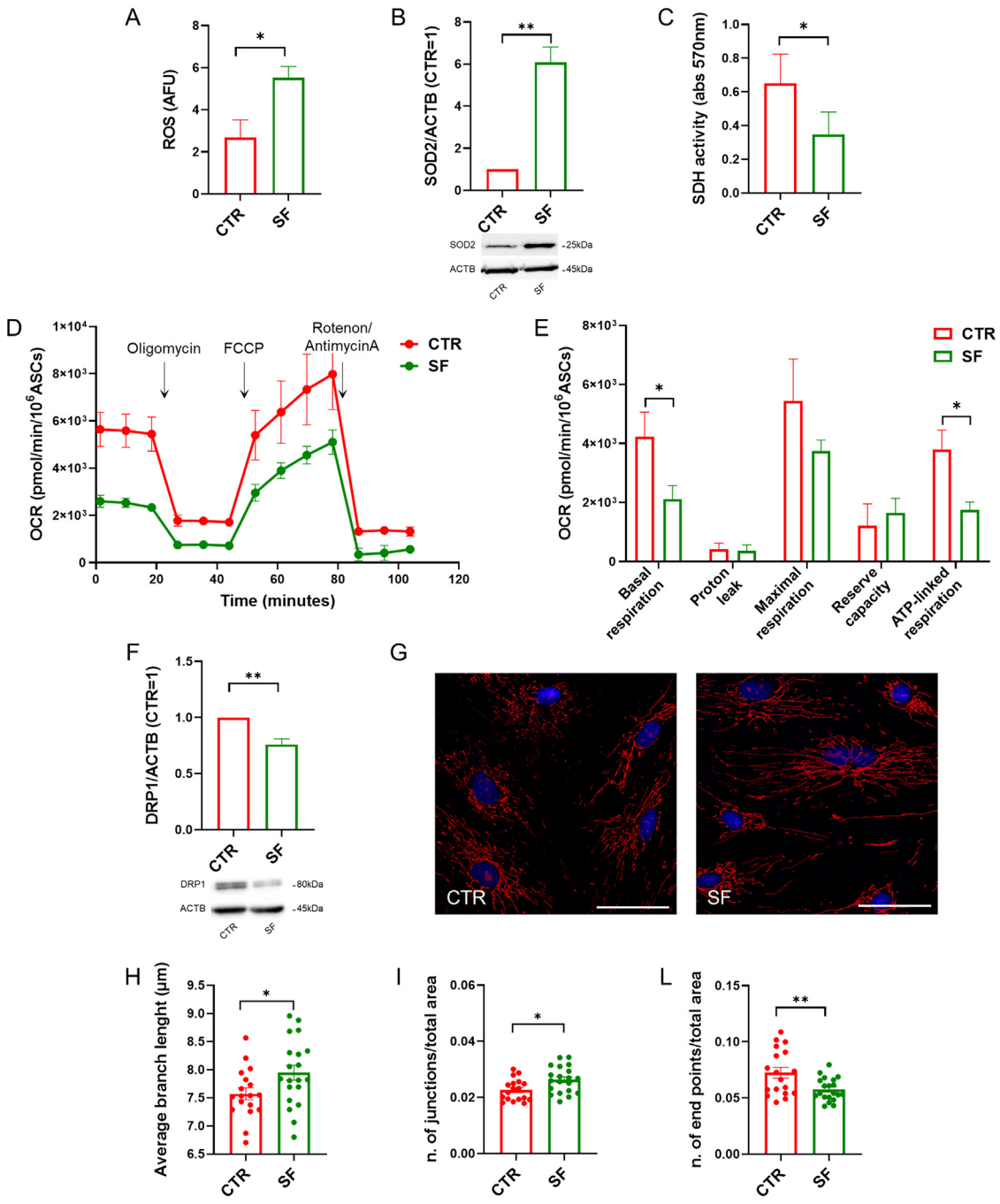

Fig. 3. Impact of serum starvation on mitochondria. (A) Intracellular ROS production by CTR and SF ASCs. Data are expressed as arbitrary fluorescence units (AFU) and represented as mean ± standard deviation (SD) of n = 5 independent experiments. (B) Mitochondrial superoxide dismutase (SOD2) expression by western blot. Data are expressed as relative values (CTR = 1) of the ratio between SOD2 and the housekeeping protein β-actin (ACTB), and represented as mean ± SD of n = 5 independent experiments. A representative membrane showing the upregulation of SOD2 expression by SF cells is reported. (C) Measurement of succinate dehydrogenase (SDH) activity in CTR and SF ASCs by MTT assay. Data are expressed as absorbance at 570 nm and represented as mean ± SD of n = 3 independent experiments. (D) OCR of CTR and SF ASCs by Seahorse assay. Data are expressed as pmol O_2/min per million cells and represented as mean ± SD of n = 3 independent experiments. Arrows indicate the sequential injection of mitochondrial inhibitors or uncouplers. (E) Basal respiration, proton leak, maximal respiration, reserve capacity and ATP-linked respiration net of non-mitochondrial respiration obtained from OCR analysis. (F) Dynamin-related protein-1 (DRP1) expression by western blot. Data are expressed as relative values (CTR = 1) of the ratio between DRP1 and ACTB, and represented as mean ± SD of n = 5 independent experiments. A representative membrane showing the down modulation of DRP1 expression by SF cells is reported. (G) Mitotracker staining of CTR and SF ASCs. Scale bars represent 50 μm. (H-L) Analysis of mitochondrial network morphology. Differences in average branch lengths (H), number of junctions (I) and end points (L) are expressed as mean ± SD of n = 2 independent experiments (20 images/group). Statistics was performed by paired (A-F) or unpaired (H-L) *t* test. Statistical significance is shown as $^{*}P < 0.05$ and $^{**}P < 0.01$.

FGF21 under CTR and SF conditions, is required to elucidate this aspect.

Mitochondrial dysfunction is also confirmed by the analysis of OCR, which resulted lower is starved cells. However, despite a significant reduction of basal and ATP-linked respiration, SF ASCs preserve their ability to face energy demand. We ascribe this feature to the enhanced complexity of their mitochondrial network. In fact, mitochondrial elongation has been already shown to protect these organelles from both serum and nutrient starvation, preserving ATP production [41].

In conclusion, we show that 72-h serum deprivation, a convenient approach to obtain ASC CM, does not induce changes in cell phenotype while it affects cell metabolism by modifying mitochondrial activity and inducing oxidative stress. We hypothesize that the stress induced by serum starvation can be involved in the release of multiple bioactive factors that can exert their pro-angiogenic, trophic and antioxidant effects.

With this study, we took a step forward in the process of characterizing MSCs in the perspective of optimizing their clinical use. However, it is mandatory to acknowledge that, despite the abundance of encouraging pre-clinical evidence, a large percentage of MSC-based clinical trials still fail to meet expectations [42]. The main challenges in the clinical translation of MSC-based therapies are linked to the lack of standardized protocols and effective quality controls, affecting the consistency of MSC properties among studies [42]. Indeed, the quality of MSCs (or their derivatives) depends on both donor-related factors, such as age, medical history and genetic traits, and technical ones, such as harvesting site, isolation procedure and *in vitro* expansion [43]. Recently, strategies based on the use of induced pluripotent stem cell-derived MSCs have emerged [44,45]. These approaches allow overcoming the issues of interdonor variability and scalability, and they may represent a promising alternative to the use of primary MSCs.

Author Contributions

Conception and design of the study: CG, SN and ATB. Acquisition of data: CG, SN, EDM, SRC and CDP. Analysis and interpretation of data: CG, SN, EDM, SRC, CDP and ATB. Drafting or revising the manuscript: CG, SN, EDM, SRC, CDP and ATB. All authors have approved the final article.

Declaration of Competing Interest

The authors have no commercial, proprietary or financial interest in the products or companies described in this article.

Acknowledgments

The authors would like to thank Dr. Rossella Daniela Bengalli (University of Milano-Bicocca) and Dr. Donatella Lattuada (University of Milan) for their valuable support with cytofluorimetry, Silvia Mary Pickering for English editing, Dr. Cristina Ruberti (cristina.ruberti@unimi.it) and the Advanced Technology Facility (Department of Biosciences, University of Milan) for the precious help with Seahorse assay. The PhD student Silvia Rosanna Casati was supported by the PhD program in Experimental Medicine of the University of Milan.

Funding

This research was funded by Italian Ministry of Health (Ricerca Corrente L1038 and L1039, IRCCS Istituto Ortopedico Galeazzi) and University of Milan, Department of Biomedical, Surgical and Dental Sciences (RV_PRO_RIC16ABRIN_M).

Supplementary materials

Supplementary material associated with this article can be found, in the online version, at doi:10.1016/j.jcyt.2023.03.004.

All data used to support the findings of this study are uploaded in zenodo repository (https://zenodo.org/record/7729082#.ZA82khWZNPZ).

References

[1] Zuk PA, et al. Multilineage cells from human adipose tissue: implications for cell-based therapies. Tissue Eng 2001;7:211–28.

[2] Srinivasan A, et al. Strategies to enhance immunomodulatory properties and reduce heterogeneity in mesenchymal stromal cells during ex vivo expansion. Cytotherapy 2022;24:456–72.

[3] Vasanthan J, et al. Role of human mesenchymal stem cells in regenerative therapy. Cells 2020;10.

[4] Chang C, et al. Effects of mesenchymal stem cell-derived paracrine signals and their delivery strategies. Adv Healthc Mater 2021;10:e2001689.

[5] Ferreira JR, et al. Mesenchymal stromal cell secretome: influencing therapeutic potential by cellular pre-conditioning. Front Immunol 2018;9:2837.

[6] Phelps J, Sanati-Nezhad A, Ungrin M, Duncan NA, Sen A. Bioprocessing of mesenchymal stem cells and their derivatives: toward cell-free therapeutics. Stem Cells Int 2018:9415367. 2018.

[7] Vu BT, Le HT, Nguyen KN, Van Pham PHypoxia. Serum starvation, and TNF-α can modify the immunomodulation potency of human adipose-derived stem cells. Adv Exp Med Biol 2021.

[8] Jung PY, et al. Adipose tissue-derived mesenchymal stem cells cultured at high density express IFN-β and TRAIL and suppress the growth of H460 human lung cancer cells. Cancer Lett 2019: 202–10. 440-441.

[9] Haraszti RA, et al. Serum deprivation of mesenchymal stem cells improves exosome activity and alters lipid and protein composition. iScience 2019;16:230–41.

[10] Oskowitz A, McFerrin H, Gutschow M, Carter ML, Pochampally R. Serum-deprived human multipotent mesenchymal stromal cells (MSCs) are highly angiogenic. Stem Cell Res 2011;6:215–25.

[11] Bakopoulou A, et al. Angiogenic potential and secretome of human apical papilla mesenchymal stem cells in various stress microenvironments. Stem Cells Dev 2015;24:2496–512.

[12] Hahm J, Kim J, Park J. Strategies to enhance extracellular vesicle production. Tissue Eng Regen Med 2021;18:513–24.

[13] Binder BY, Sagun JE, Leach JK. Reduced serum and hypoxic culture conditions enhance the osteogenic potential of human mesenchymal stem cells. Stem Cell Rev Rep 2015;11:387–93.

[14] Kim JH, Shin SH, Li TZ, Suh H. Influence of in vitro biomimicked stem cell 'niche' for regulation of proliferation and differentiation of human bone marrow-derived mesenchymal stem cells to myocardial phenotypes: serum starvation without aid of chemical agents and prevention of spontaneous stem cell transformation enhanced by the matrix environment. J Tissue Eng Regen Med 2016;10:E1–13.

[15] Brini AT, et al. Therapeutic effect of human adipose-derived stem cells and their secretome in experimental diabetic pain. Sci Rep 2017;7:9904.

[16] Niada S, Giannasi C, Gualerzi A, Banfi G, Brini AT. Differential proteomic analysis predicts appropriate applications for the secretome of adipose-derived mesenchymal stem/stromal cells and dermal fibroblasts. Stem Cells Int 2018:7309031. 2018.

[17] Niada S, et al. Adipose-derived stromal cell secretome reduces TNFalpha-induced hypertrophy and catabolic markers in primary human articular chondrocytes. Stem Cell Res 2019;38:101463.

[18] Giannasi C, et al. Comparison of two ASC-derived therapeutics in an in vitro OA model: secretome versus extracellular vesicles. Stem Cell Res Ther 2020;11:521.

[19] Niada S, Giannasi C, Magagnotti C, Andolfo A, Brini AT. Proteomic analysis of extracellular vesicles and conditioned medium from human adipose-derived stem/stromal cells and dermal fibroblasts. J Proteomics 2020;232:104069.

[20] Carlomagno C, et al. Raman fingerprint of extracellular vesicles and conditioned media for the reproducibility assessment of cell-free therapeutics. Front Bioeng Biotechnol 2021;9:640617.

[21] Amodeo G, et al. Secretome of human adipose-derived mesenchymal stem cell relieves pain and neuroinflammation independently of the route of administration in experimental osteoarthritis. Brain Behav Immun 2021;94:29–40.

[22] Giannasi C, et al. Towards secretome standardization: identifying key ingredients of MSC-derived therapeutic cocktail. Stem Cells Int 2021;2021:3086122.

[23] Showalter MR, et al. Primed mesenchymal stem cells package exosomes with metabolites associated with immunomodulation. Biochem Biophys Res Commun 2019;512:729–35.

[24] Rose S, et al. Oxidative stress induces mitochondrial dysfunction in a subset of autism lymphoblastoid cell lines in a well-matched case control cohort. PLoS One 2014;9:e85436.

[25] Baer PC, Geiger H. Adipose-derived mesenchymal stromal/stem cells: tissue localization, characterization, and heterogeneity. Stem Cells Int 2012;2012:812693.

[26] Wan Safwani WK, et al. The effects of hypoxia and serum-free conditions on the stemness properties of human adipose-derived stem cells. Cytotechnology 2016;68:1859–72.

[27] Chen M, et al. Serum starvation induced cell cycle synchronization facilitates human somatic cells reprogramming. PLoS One 2012;7:e28203.

[28] Leontieva OV, Demidenko ZN, Blagosklonny MV. Contact inhibition and high cell density deactivate the mammalian target of rapamycin pathway, thus suppressing the senescence program. Proc Natl Acad Sci U S A 2014;111:8832–7.

[29] Majumdar D, Bhonde R, Datta I. Influence of ischemic microenvironment on human Wharton's jelly mesenchymal stromal cells. Placenta 2013;34:642–9.

[30] Zeidler JD, et al. Short-term starvation is a strategy to unravel the cellular capacity of oxidizing specific exogenous/endogenous substrates in mitochondria. J Biol Chem 2017;292:14176–87.

[31] Rambold AS, Kostelecky B, Elia N, Lippincott-Schwartz J. Tubular network formation protects mitochondria from autophagosomal degradation during nutrient starvation. Proc Natl Acad Sci U S A 2011;108:10190–5.

[32] Tretter L, Patocs A, Chinopoulos C. Succinate, an intermediate in metabolism, signal transduction, ROS, hypoxia, and tumorigenesis. Biochim Biophys Acta 2016;1857:1086–101.

[33] Lee SB, et al. Serum deprivation-induced reactive oxygen species production is mediated by Romo1. Apoptosis 2010;15:204–18.
[34] Liu SY, et al. Albumin prevents reactive oxygen species-induced mitochondrial damage, autophagy, and apoptosis during serum starvation. Apoptosis 2012;17:1156–69.
[35] Agrahari G, Sah SK, Kim TY. Superoxide dismutase 3 protects mesenchymal stem cells through enhanced autophagy and regulation of FoxO3a trafficking. BMB Rep 2018;51:344–9.
[36] Zheng J, et al. Leptin protects cardiomyocytes from serum-deprivation-induced apoptosis by increasing anti-oxidant defence. Clin Exp Pharmacol Physiol 2010;37:955–62.
[37] Chiaradia E, et al. Extracellular vesicles under oxidative stress conditions: biological properties and physiological roles. Cells 2021;10.
[38] Scholle LM, Lehmann D, Deschauer M, Kraya T, Zierz S. FGF-21 as a potential biomarker for mitochondrial diseases. Curr Med Chem 2018;25:2070–81.
[39] Suomalainen A, et al. FGF-21 as a biomarker for muscle-manifesting mitochondrial respiratory chain deficiencies: a diagnostic study. Lancet Neurol 2011;10:806–18.
[40] Kliewer SA, Mangelsdorf DJ. A dozen years of discovery: insights into the physiology and pharmacology of FGF21. Cell Metab 2019;29:246–53.
[41] Gomes LC, Di Benedetto G, Scorrano L. During autophagy mitochondria elongate, are spared from degradation and sustain cell viability. Nat Cell Biol 2011;13:589–98.
[42] Zhou T, et al. Challenges and advances in clinical applications of mesenchymal stromal cells. J Hematol Oncol 2021;14:24.
[43] Lukomska B, et al. Challenges and controversies in human mesenchymal stem cell therapy. Stem Cells Int 2019:9628536. 2019.
[44] Lian Q, Zhang Y, Liang X, Gao F, Tse HF. Directed differentiation of human-induced pluripotent stem cells to mesenchymal stem cells. Methods Mol Biol 2016;1416:289–98.
[45] Bloor AJC, et al. Production, safety and efficacy of iPSC-derived mesenchymal stromal cells in acute steroid-resistant graft versus host disease: a phase I, multicenter, open-label, dose-escalation study. Nat Med 2020;26:1720–5.